CRYSTAL GROWTH & DESIGN

pubs.acs.org/crystal

Article

Ripening of Gold Clusters into a Single Domain on Semiconductor Quantum Rods during Langmuir–Blodgett Deposition

Xiao Tang and Xiaohang Li*

Cite This: *Cryst. Growth Des.* 2020, 20, 5890–5895

Read Online

ACCESS | Metrics & More | Article Recommendations | Supporting Information

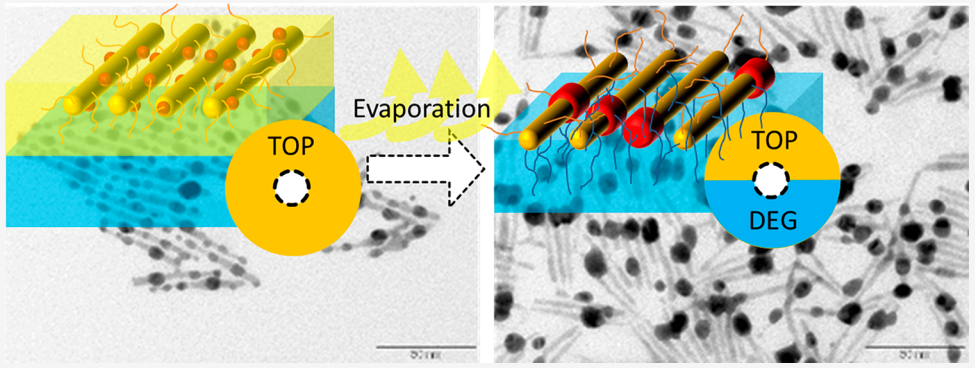

ABSTRACT: Rapidly forming, large gold nanocrystals (~10 nm) on CdSe/CdS nanorods while maintaining the nanorod geometry remains challenging. In this study, we demonstrate that by using Langmuir–Blodgett (LB) deposition, numerous tiny gold nanocrystals (2–3 nm) can ripen into a single gold nanocrystal with a size of 8–9 nm on each nanorod within 4 h. Thanks to the room temperature condition and low corrosiveness of the chemicals used in the technique, the nanorod geometry was perfectly maintained. Besides, the reaction was found to be accompanied by a ligand exchange procedure, which perhaps resulted in a hydrophobic/hydrophilic "Janus" structure on the final hybrid nanoparticles.

1. INTRODUCTION

Colloidal inorganic nanocrystals (NCs), including but not limited to nanosized semiconductors (e.g., CdS, ZnSe, ZnO, etc.), magnetite (e.g., CoPt, Fe_2O_3, etc.), or metal-based composite particles (e.g., Ag, Au, Al, etc.), have long attracted considerable attention in the past two decades owing to their unique functions such as fluorescence, magnetism, and surface plasmon resonance.[1−8] Furthermore, heterostructures, by assembling multiple NCs joined into a unique particle, would provide enhanced or multiple properties and capabilities.[9−13] Particularly, hybrid nanoparticles (HNPs), by combining semiconductor NCs (SNCs) and noble metal NCs (MNCs) in close vicinity, may show enhanced absorption cross-section, charge transfer, or photoluminescence in comparison to SNCs alone.[9,10,14−16] Hence, such HNPs are promising in potential applications such as biological imaging, photodetection, photovoltaics, and so on.[9,14] Specifically, among the SNCs, elongated one dimensional (1D) CdSe/CdS core/shell nanorods (NRs) received the most intensive investigation since they show a tunable bandgap in the visible light spectrum and stable and relatively high photoluminescence (PL) with monoexponenital PL decay dynamics;[17−19] for the MNCs, gold MNCs are the most popular one since they show tunable plasmonic resonances in the visible light spectrum together with high biocompatibility and high reproducibility.[5] As a result, CdSe/CdS/gold HNPs have set an ideal research model for manipulating semiconductor/plasmonic interactions.[9,10]

It is known that the interaction between CdSe/CdS core/shell SNCs and gold MNCs dominantly depends on the nanocrystal size, shape, and composition of each of them. Nowadays, fabrication of nanometric spheres, rods, tetrapods, tripods, and other shapes of various SNCs has been developed into a fairly mature technology.[9,14] Besides, the geometry and size of both metal spheres and rods can also be well-tailored in the nanoscale.[14,20,21] Therefore, a straightforward strategy for accurate control over the size and geometry of each component of the hybrid particle is via direct attachment of preformed SNCs and MNCs that already have the desired geometry. In this strategy, the preformed SNCs or MNCs need to be coated with desired polymers with functional peptides which are positively or negatively charged, respectively (vice

Received: April 29, 2020
Revised: June 7, 2020
Published: July 30, 2020

versa). Then, such preformed NCs with opposite charges can be naturally conjugated via electrostatic forces.[22−25] In most cases, this route is only performable in a water environment since the electrostatic force can only be manipulated in polar solvents.[25] Therefore, it usually requires an additional ligand transfer procedure to make the oil-processed NCs water-compatible. For this reason, such a conjugating route is fairly complicated and time-consuming.[25] Moreover, for the MNCs and SNCs preformed separately by using different organic ligands, the as-prepared NCs usually show an intrinsic difference in solubility or/and stability in a specific solvent. This would either weaken the combination between the MNCs and SNCs in the final hybrid particles or result in uncontrollable large-scale agglomeration between many of them.[9,25,26] In this consideration, direct in situ growth of gold MNCs on CdSe/CdS NRs as templates forming HNPs appears to be an alternative strategy.[9,10,15,27] Along this, a model synthesis technology was developed by Mokari et al. and in general can be divided into two steps: the conventional fabrication of CdSe/CdS NRs in phosphoric fatty compound and then the reduction of precursor Au^{3+} ions followed by the consequent nucleation and growth of gold MNCs on the surface of NRs.[16] Indeed, such in situ synthesis technique is more facile in contrast to the aforementioned conjugation method. Nevertheless, it suffers from two main disadvantages: first, the size of the in situ grown gold MNCs is usually limited in the range of 1−2 nm. The underlying electrochemical Ostwald ripening is a rather slow process;[27] it requires several days to approach 10 nm, which is however fairly close the minimum size for gold to show surface plasmon resonance. To solve this problem, the in situ gold growth process can be modified either by elevating the reaction temperature or utilizing ultraviolet (UV) irradiation as a catalyst.[27,28] However, all these methods can be harmful to the structure and optical performance of the CdSe/CdS NRs. It is actually relating to another disadvantage: because of the fragility of CdSe/CdS, the NRs can shrink significantly in length during the growth of anchored gold MNPs.[10]

In this report, we demonstrate that the ripening growth of the gold MNCs anchored on CdSe/CdS NRs can be largely facilitated by using Langmuir−Blodgett (LB) deposition. Such a technique requires neither UV light catalyst nor high temperature. In the experiment, numerous tiny (2−3 nm) gold MNCs first nucleate on the surface of the NRs to form the initial HNPs by immersing the NRs in toluene-Au^{3+} precursor. Then, the as-prepared toluene dispersion of HNPs that was floating spread on the top of diethylene glycol (DEG) that was contained in a LB basin. With the barriers in the LB device moving forward to each other, the area of the floating toluene dispersion of HNPs shrinks gradually. During this procedure, gold MNCs can grow into 8−9 nm within 4 h at room temperature. We also found that the growth of gold MNCs was accompanied by a ligand exchange procedure, which perhaps results in a hydrophobic/hydrophilic "Janus" structure on the final hybrid NPs. Moreover, thanks to the room temperature and low corrosiveness of the chemicals used in the technique, the resulting HNPs show no significant shrinkage in the length of the NRs. We believe that this novel technique is also promising for growing other kinds of heterogeneous structures in which the components need to reach specific sizes.

2. EXPERIMENTAL SECTION

2.1. Synthesis of CdSe/CdS NRs. Prior to the combination with gold MNCs, CdSe/CdS core/shell NRs were synthesized via a conventional wet-chemistry method that can be found elsewhere.[29] First of all, a mixture of octadecylphosphonic acid (ODPA) (0.29 g) and trioctylphosphine oxide (TOPO) (3.0 g), together with CdO (0.051 g), was placed in a three-neck flask. In order to remove the crystallized water, the flask was heated up to 110 °C and held for 1 h under a vacuum. Then, purging with nitrogen, the flask was further heated to 300 °C. The temperature was held for 10 min to completely complex the cadmium with TOPO and OPDA. In another vial, selenide was dissolved in 1.6 mL of tributylphosphine (TOP) forming a 0.5 M solution. Such a solution was loaded in a syringe and injected into the flask when temperature decreased to 250 °C. After a 3 min holding period at 250 °C, the flask was rapidly cooled to room temperature, followed by an injection of 10 mL of methanol. After multiple times of centrifugation at 7000 rpm for 5 min and washing with a mixture of toluene and methanol, the collected cores were finally dispersed in TOP (5 mL). By utilizing the method explained by Yu et al., 0.35 mM and 3.5 nm were determined as the concentration and the size of the quantum dots, respectively.[30] After the calculation, the dispersion was then placed in a glovebox under inert atmosphere.

On the basis of such TOP dispersion of CdSe cores, the CdS shell was grown as described in the following. Similar to the first step that was described for the synthesis of CdSe cores, a mixture of TOPO (3 g) and hexylphosphonic acid (0.08 g), together with CdO (0.086 g), was placed in a three-neck flask. Also, crystallized water had to be removed before triggering the reaction. Then purging with nitrogen, the flask was slowly heated up until 370 °C. In the meantime, sulfur was dissolved in TOP to form a 2 M solution. The aforementioned CdSe dispersion (0.8 mL), pure TOP (0.6 mL), and sulfur-TOP solution were loaded in syringes and consequently injected into the flask when temperature decreased to 350 °C. After a 6 min holding period, the flask was rapidly cooled to room temperature and again followed by an injection of 10 mL of methanol. After multiple times of centrifugation at 7000 rpm for 5 min and washing with a mixture of toluene and methanol, the collected CdSe/CdS core/shell NRs were finally dispersed in toluene (10 mL).

2.2. Synthesis of CdSe/CdS/Au HNPs. First of all, $HAuCl_4$ (10 mg) was dissolved in 1 mL of toluene with the help of 100 μL of oleylamine. In another vial, 50 μL of the as-prepared toluene dispersion of CdSe/CdS NRs was diluted to 2 mL by adding additional toluene. The $HAuCl_4$ solution and the NRs dispersion were mixed in a three-neck flask and heated up to 50 °C and held for 5 h under nitrogen flow. Finally, 10 mL of methanol was added to precipitate the CdSe/CdS/Au HNPs. The as-prepared CdSe/CdS/Au HNPs were separated by centrifugation at 11 000 rpm and finally dispersed in 500 μL of toluene for use.

2.3. LB Deposition. Before the deposition was carried out, a KSV Nima KN-2002 system was thoroughly cleaned with isopropyl alcohol for at least three times. After cleaning, the basin was filled with DEG as a subphase. Then a transmission electron microscopy (TEM) grid was mounted onto the workshop-made sample holder of the dipper, followed by dipping into DEG. By using a microliter glass syringe, the aforementioned toluene dispersion of HNPs was slowly spread out onto the surface of DEG to form a homogeneous floating layer. The floating layer was then slowly compressed at a constant rate of 1 mm/min until the desired target pressure was achieved. After the compression process, the TEM grid was lifted up at a rate of 1 mm/min. Finally, the grid was placed in a vacuum oven to allow it completely dry at room temperature overnight.

2.4. Characterization. TEM images, absorption spectrum, and FT-IR spectrum were measured by using a transmission electron microscope (JEOL JEM- 1011), a Cary 5000 UV−vis-NIR spectrophotometer, and a Varian 660 FTIR spectrophotometer, respectively.

https://dx.doi.org/10.1021/acs.cgd.0c00582
Cryst. Growth Des. 2020, 20, 5890−5895

3. RESULTS AND DISCUSSION

Figure 1a,c,e shows TEM images of (a) the initial CdSe/CdS/Au HNPs (before LB deposition), (b) the HNPs quenched during LB deposition when the surface pressure reaches at 8 mN·m, and (c) the HNPs obtained after LB deposition, that is, when the surface pressure reaches 14 mN·m. The corresponding size distribution histograms of diameter of the gold MNCs and length of the CdSe/CdS NRs are reflected in Figure 1b,d,f. It is noted that the size distribution analysis was based on the observation of 200 MNCs for each sample; thus, TEM images obtained in a larger scale that contain more MNCs are shown in Figure 1Sa–c (Supporting Information), respectively. First of all, Figure 1a shows that after being immersed in a $HAuCl_4$–oleylamine precursor solution, the CdSe/CdS NRs were all decorated with multiple tiny gold clusters. Such a structure is consistent with that reported by van Huis et al.[31] The mechanism of the anchoring and the reduction of Au^{3+} ions on the surface of CdS nanorods is believed due to the higher stability of Au_xS_y in comparison to CdS. Then, during the LB deposition, an electrochemical ripening process takes place, in which a single large gold MNC forms on each original host NR at the expense of the tiny ones. Such a tendency is evidenced by the increase in the average size of the MNCs (from 2.87 nm (b) to 8.25 nm (f)) together with the decrease in the average number of the MNCs on each NR (from ~6 (a) to 1 (e)). Besides, different from the previous reports in which NRs was found to have shrunk significantly in length with the growth of anchored MNCs, in our research, the length of the NRs was found to be largely preserved as reflected from the average size of the NR before (41.75 nm (b)) and after the LB deposition (39.96 nm (f)).[16] This can be first attributed to the room temperature for LB deposition and second to the neglectable corrosiveness of DEG compared to the previously used organobromine compounds. Moreover, the TEM images show that majority of the HNPs were self-organized in bundle arrays with a visible and uniform distance between individuals. It means throughout the LB deposition process, the HNPs are persistently covered with surface ligands, which effectively provide a repulsive steric force to prevent hydrogen-bonding induced, uncontrollable large-scale aggregation. To the best of our knowledge, such self-assembly behavior is commonly observed in oil-phase prepared CdSe/CdS NRs; however it becomes fairly challenging to maintain if the NRs are decorated with additional domains (such as metal and silica) according to previous publications.[16,27,30,32] This is likely due to the disordering or partial loss of the original compactly arranged capping ligands during further chemical reactions.

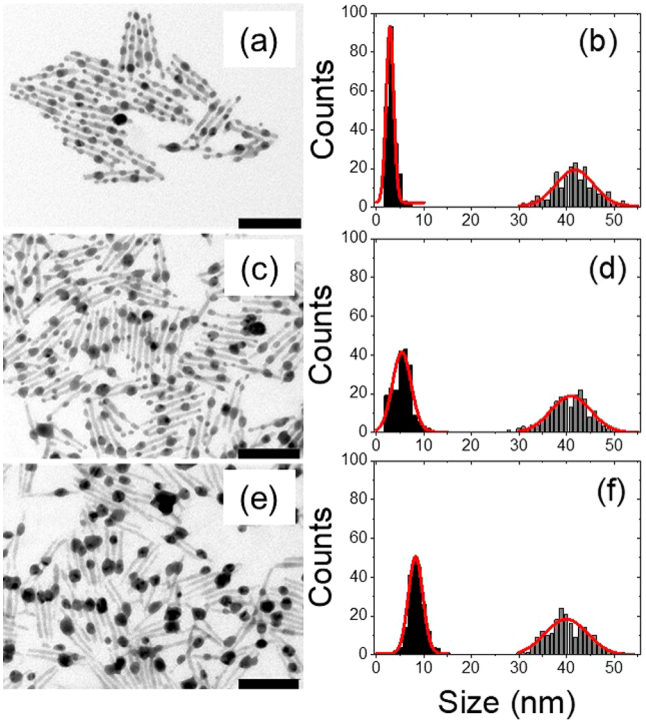

Figure 1. TEM images and the corresponding size distribution histograms (the black columns show the diameter distribution of the gold NPs, and the gray columns show the length distribution of the NRs; the red curves were generated by Gaussian fitting based on each of them) of (a, b) the initial CdSe/CdS/Au HNPs (before LB deposition), (c, d) the HNPs quenched during LB deposition when the surface pressure reaches at 8 mN·m, and (e, f) the HNPs obtained after LB deposition when the surface pressure reaches 14 mN·m. The scale bar for the TEM images is 50 nm.

To track the evolution of capping ligands on the CdSe/CdS/Au HNPs throughout the reaction, FTIR spectroscopy was performed on the samples (i) before and (ii) after LB deposition, together with (iii) the pure DEG as a reference, as shown in Figure 2. It is noted that before the measurements, samples (i) and (ii) were all washed with methanol multiple times in order to thoroughly remove the excess ligands and solvents. For the HNPs before LB deposition (spectrum (i)), the most prominent vibration peaks are observed at 2956, 2923, and 2854 cm^{-1}, which can be assigned to the asymmetric stretching vibration mode of CH_3, asymmetric, and symmetric stretching vibration modes of CH_2, respectively; two less prominent peaks take place at 1492 and 1463 cm^{-1}, which can be assigned to the asymmetric in-plane and symmetric rocking mode of CH_3, respectively; also, cluster peaks are observed at around 1082 cm^{-1}, which can be assigned to the P═O stretch. Evidently, all the vibration peaks observed here are the characteristic modes of phosphonic acids including TOPO, TOP, and ODPA used during synthesis of CdSe/CdS core/shell SNCs. This finding is in good agreement with previous reports published elsewhere.[33,34] However, the spectrum does not show any typical characteristics of amine groups such as the potential peaks at 1576 and 3300 cm^{-1} that correspond to the NH_2 scissoring mode and the ν (N–H) stretching mode,

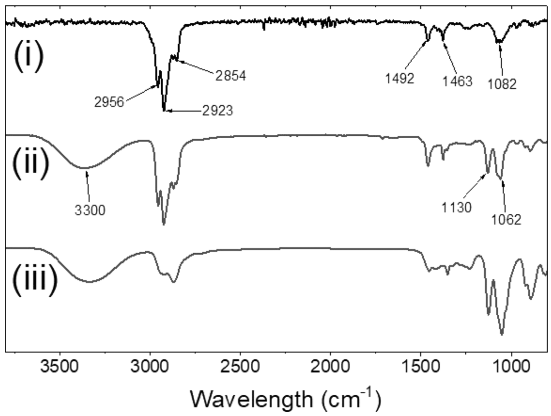

Figure 2. FT-IR spectra of CdSe/CdS/Au HNPs (i) before and (ii) after LB deposition, and (iii) pure DEG.

https://dx.doi.org/10.1021/acs.cgd.0c00582
Cryst. Growth Des. 2020, 20, 5890–5895

respectively. It means although oleylamine was used as a stabilizer for Au^{3+} ions during the initial gold cluster attachment on the surface of CdSe/CdS core/shell SNCs, all (or at least majority) of them did not passivate or reside on the surface of SNCs but were removed through the washing process. For the spectrum obtained on sample (ii), a new wide band centered at 3300 cm^{-1} appears. Besides, the aforementioned cluster peaks centered at around 1082 cm^{-1} saw an obvious splition together with a significant increased relative intensity with respect to that of the methyl-group generated vibration peaks at around 3000 cm^{-1}. In order to understand the origination of such a difference between sample (i) and (ii), the spectrum was also obtained on the pure DEG (iii). On the basis of the spectrum of DEG, it is undoubtable that the wide band centered at 3300 cm^{-1} in sample (ii) is attributed to the −OH vibration of DEG. Besides, the enhanced intensity in the cluster peaks at around 1082 cm^{-1} also highly likely originates from the added peaks in DEG, which correspond to the $-CH_2-O-CH_2-$ band. More importantly, it can be seen that spectrum (ii) is neither completely the same as (i) nor (iii), in terms of the ratio of the intensity of the peaks at around 3000 cm^{-1} to that at around 1082 cm^{-1}. Instead, spectrum (ii) appears as a merging of (i) and (iii), indicating a coexistence of phosphonic acid and DEG ligands after LB deposition. Such a phenomenon is in good agreement with previous reports, in which people believe that nanoparticles can transform to a "Janus"-like structure when trapped at the water/oil (or air/oil) interface by partially exchanging their covered ligand.[35,36]

On the basis of the above discussion, the mechanism for the gold ripening growth is summarized and schematically illustrated in Figure 3. Initially, toluene-dispersed CdSe/CdS/Au HNPs was stabilized by TOPO/TOP. When the dispersion of HNPs was added dropwise to the surface of DEG, the HNPs remained suspended in the toluene phase floating on the top of DEG. Therefore, the surface of the HNPs was still homogeneously covered with the hydrophobic phosphonic acids. With the evaporation of toluene, the vicinity environment of the HNPs rapidly evolved from an oil/DEG interface to an air/DEG interface. Then, the hydrophobic phosphonic acids that attached on the bottom part of the HNP surface were exchanged by DEG ligands spontaneously. Similar processes have been proven energetically favorable because they can decrease the interfacial energy between the HNPs and DEG.[37,38] Since then, the original hydrophobic HNPs were changed into hydrophobic/hydrophilic "Janus" structures which allow them to float stably on the surface of DEG.[39]

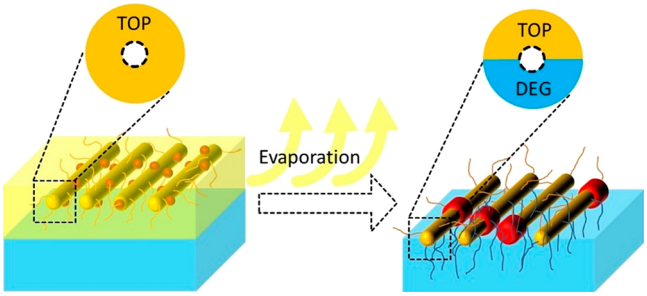

Figure 3. Schematic representation of the gold MNC ripening and the ligand exchange behavior on the NRs during LB deposition upon toluene evaporation.

Together with the ligand exchange process, the original tiny gold MNCs ripened into a larger single gold MNC on each host NR. Indeed, there exists one argument: if it is possible that the ripening of tiny gold MNCs takes place not only on individual host NRs but also happens between multiple adjacent ones. If this is the case, there should be a noticeable number of empty NRs that lost all their original tiny MNCs during the ripening process. In consideration, we counted the number of large gold NPs and also the number of NRs in Figure 1e. The ratio of the number of MNCs to that of NRs was found indeed close to 1, and therefore we believe that the tiny gold MNCs, which serve as the ripening source, only migrate along their original host NRs. Besides, it is crucial to clarify the relation between the gold ripening and the ligand exchange processes that both took place during the LB deposition. Hence, a controlling experiment was performed by simply mixing 500 μL of toluene dispersion of the initial CdSe/CdS/Au HNPs and 500 μL of DEG in a closed glass vial under vigorous stirring (that is, without using LB deposition, thus also without toluene evaporation). Similar reaction processes, usually named as a "bi-phase" ligand exchange reaction, can be found elsewhere.[39,40] After 72 h of stirring, the HNPs were washed with methanol multiple times and then finally dispersed in methanol for TEM and FT-IR measurements, which are shown in Figure 4, panels a and b, respectively. The TEM image indicates that even after a much longer reaction time (72 h) compared to that used in LB deposition (4 h), no visible ripening of gold MNCs happened on the NRs. However, the FT-IR shows that the spectrum taken on the sample was exactly the same as that of pure DEG (Figure 2 (ii)), implying that all of the original TOP/TOPO ligands were completely substituted by DEG. First, the controlling experiments suggest that the ligand exchange can be a transit process when the surface of HNPs is exposed to DEG atmosphere and is much faster and easier with respect to the gold ripening. Second, assuming that the ligand exchange

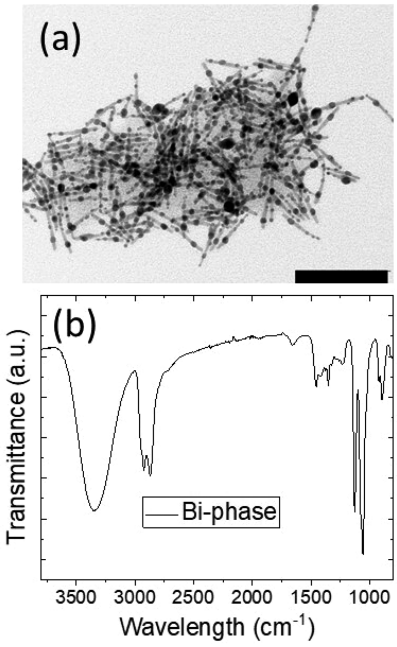

Figure 4. TEM image (a) and FT-IR spectrum (b) of the controlling sample. The scale bar for the TEM image is 100 nm.

https://dx.doi.org/10.1021/acs.cgd.0c00582
Cryst. Growth Des. 2020, 20, 5890−5895

process is fast and easy, the FT-IR spectrum shown in Figure 2 (ii) is more likely due to a complete substitution only on the bottom surface of the NRs, rather than a partial substitution around the whole surface. Therefore, it supports the assumed formation of a "Janus" structure. Third, in the LB deposition the HNPs are entrapped at the air/DEG interface, while in the "bi-phase" controlling experiment, the MNCs are entrapped at the toluene/DEG interface. It is therefore deduced that the air/DEG interface plays the key role in triggering the MNC ripening process by enhancing the mobility of the tiny MNCs along the longitudinal direction of the NRs.

Absorption was carried out to study the effect of Au ripening on the optical properties of the HNPs. Figure 5 shows the

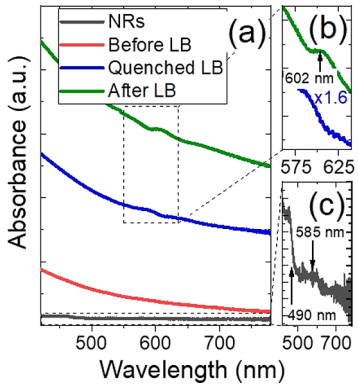

Figure 5. (a) Absorbance spectrum of the neat CdSe/CdS NRs (black), the initial CdSe/CdS/Au HNPs before LB deposition (red), the HNPs quenched during LB deposition when the surface pressure reaches 8 mN·m and (blue), and the HNPs obtained after LB deposition (green); (b) zoomed absorbance plots of the neat CdSe/CdS NRs in the 430−780 nm wavelength range; (c) zoomed absorbance plots of the initial CdSe/CdS/Au HNPs quenched during LB deposition and the HNPs after LB deposition in the 430−780 nm wavelength range.

absorbance spectrum of the neat CdSe/CdS NRs (black), the initial CdSe/CdS/Au HNPs before LB deposition (red), the HNPs quenched during LB deposition when the surface pressure reaches at 8 mN·m and (blue), and the HNPs obtained after LB deposition (green). Absorption band from CdSe-core (585 nm) and CdS-shell (490 nm) is only visible together in the neat NRs sample, as shown in Figure 5b. Upon attachment of the tiny gold MNCs, the absorbance in the visible spectrum is largely enhanced together with a complete disappearance of all the absorption characteristics of the neat NRs. With an increase of the gold MNCs during LB deposition, the absorbance in the visible spectrum is further enhanced, with absorption band at around 600 nm gradually emerging, as shown in Figure 5c. However, we notice that the average size of gold MNCs reaches 8 nm after LB deposition (Figure 1e,f), which in principle cannot solely give rise to a surface plasmon resonance at 600 nm.[5] According to previous reports that deal with similar gold-NR hybrid structures, the spectrum observed here may not reflect a simple sum of spectra from gold and NR. Instead, it reflects a modified electronic structure of the metal−semiconductor mixed system, which usually exhibits broadened levels and a reduced band gap.[10,16] This means that the observed weak 600 nm peak may due to a red-shifting of the surface plasmon band generated by the formed 8 nm gold MNCs.

4. CONCLUSION

We have demonstrated the formation of a gold-CdSe/CdS heterogeneous hybrid structure with the size of gold MNCs reaching 8.2 nm by utilizing the LB deposition process. During the process, originally attached tiny gold MNCs migrate along the air/DEG interface and eventually ripen into a single large gold MNC on each host CdSe/CdS NR. This is found accompanied by a ligand exchange procedure, which perhaps results in a hydrophobic/hydrophilic "Janus" structure on the final HNPs. Moreover, thanks to the room temperature condition and low corrosiveness of the chemicals used in the technique, the resulting HNPs show no significant shrinkage in the length of the NRs. We believe that this novel technique is also promising for growing other kinds of heterogeneous structures in which the components need to reach specific sizes.

■ ASSOCIATED CONTENT

Supporting Information

The Supporting Information is available free of charge at https://pubs.acs.org/doi/10.1021/acs.cgd.0c00582.

TEM images of the initial CdSe/CdS/Au HNPs (before LB deposition), the HNPs quenched during LB deposition when the surface pressure reaches 8 mN·m, and the HNPs obtained after LB deposition when the surface pressure reaches 14 mN·m (S1) (PDF)

■ AUTHOR INFORMATION

Corresponding Author

Xiaohang Li − *Advanced Semiconductor Laboratory, King Abdullah University of Science and Technology (KAUST), Thuwal 23955-6900, Saudi Arabia;* orcid.org/0000-0002-4434-365X; Email: xiaohang.li@kaust.edu.sa

Author

Xiao Tang − *Advanced Semiconductor Laboratory, King Abdullah University of Science and Technology (KAUST), Thuwal 23955-6900, Saudi Arabia;* orcid.org/0000-0002-0138-7206

Complete contact information is available at: https://pubs.acs.org/10.1021/acs.cgd.0c00582

Notes

The authors declare no competing financial interest.

■ ACKNOWLEDGMENTS

The authors acknowledge funding from King Abdullah University of Science and Technology (Baseline Fund BAS/1/1664-01-01, Competitive Research Grants URF/1/3437-01-01, and Competitive Research Grants URF/1/3771-01-01, GCC Research Council Grant REP/1/3189-01-01).

■ REFERENCES

(1) Sonnichsen, C. D.; Kipp, T.; Tang, X.; Kambhampati, P. Efficient Optical Gain in CdSe/CdS Dots-in-Rods. *ACS Photonics* **2019**, *6* (2), 382−8.

(2) Zhang, R.; Szczepaniak, S. M.; Carter, N. J.; Handwerker, C. A.; Agrawal, R. A Versatile Solution Route to Efficient Cu2ZnSn(S,Se)-4Thin-Film Solar Cells. *Chem. Mater.* **2015**, *27* (6), 2114−20.

(3) Zhang, R. H.; Slamovich, E. B.; Handwerker, C. A. Controlling growth rate anisotropy for formation of continuous ZnO thin films from seeded substrates. *Nanotechnology* **2013**, *24* (19), 195603.

(4) Amendola, V.; Bakr, O. M.; Stellacci, F. A Study of the Surface Plasmon Resonance of Silver Nanoparticles by the Discrete Dipole Approximation Method: Effect of Shape, Size, Structure, and Assembly. *Plasmonics* **2010**, *5* (1), 85−97.
(5) Amendola, V.; Pilot, R.; Frasconi, M.; Marago, O. M.; Iati, M. A. Surface plasmon resonance in gold nanoparticles: a review. *J. Phys.: Condens. Matter* **2017**, *29* (20), 203002.
(6) Lin, M.; Tan, H. R.; Tan, J. P. Y.; Bai, S. Understanding the Growth Mechanism of α-Fe2O3 Nanoparticles through a Controlled Shape Transformation. *J. Phys. Chem. C* **2013**, *117* (21), 11242−50.
(7) Gérard, D.; Gray, S. K. Aluminium plasmonics. *J. Phys. D: Appl. Phys.* **2015**, *48* (18), 184001.
(8) Sun, X.; Jia, Z. Y.; Huang, Y. H.; Harrell, J. W.; Nikles, D. E.; Sun, K.; et al. Synthesis and magnetic properties of CoPt nanoparticles. *J. Appl. Phys.* **2004**, *95* (11), 6747−9.
(9) Tang, X.; Kröger, E.; Nielsen, A.; Schneider, S.; Strelow, C.; Mews, A.; et al. Fluorescent Metal−Semiconductor Hybrid Structures by Ultrasound-Assisted in Situ Growth of Gold Nanoparticles on Silica-Coated CdSe-Dot/CdS-Rod Nanocrystals. *Chem. Mater.* **2019**, *31* (1), 224−32.
(10) Khon, E.; Mereshchenko, A.; Tarnovsky, A. N.; Acharya, K.; Klinkova, A.; Hewa-Kasakarage, N. N.; et al. Suppression of the plasmon resonance in Au/CdS colloidal nanocomposites. *Nano Lett.* **2011**, *11* (4), 1792−9.
(11) Makkar, M.; Saha, A.; Khalid, S.; Viswanatha, R. Thermodynamics of Dual Doping in Quantum Dots. *J. Phys. Chem. Lett.* **2019**, *10* (8), 1992−8.
(12) Zhang, S.; Xu, W.; Zeng, M.; Li, J.; Xu, J.; Wang, X. Hierarchically grown CdS/alpha-Fe2O3 heterojunction nanocomposites with enhanced visible-light-driven photocatalytic performance. *Dalton Trans.* **2013**, *42* (37), 13417−24.
(13) Costi, R.; Saunders, A. E.; Banin, U. Colloidal hybrid nanostructures: a new type of functional materials. *Angew. Chem., Int. Ed.* **2010**, *49* (29), 4878−97.
(14) Ji, B.; Giovanelli, E.; Habert, B.; Spinicelli, P.; Nasilowski, M.; Xu, X.; et al. Non-blinking quantum dot with a plasmonic nanoshell resonator. *Nat. Nanotechnol.* **2015**, *10* (2), 170−5.
(15) Zhang, J.; Tang, Y.; Lee, K.; Ouyang, M. Nonepitaxial Growth of Hybrid Core-Shell Nanostructures with Large Lattice Mismatches. *Science* **2010**, *327*, 1634−8.
(16) Mokari, T.; Rothenberg, E.; Popov, I.; Costi, R.; Banin, U. Selective Growth of Metal Tips onto Semiconductor Quantum Rods and Tetrapods. *Science* **2004**, *304*, 1787−90.
(17) Zhou, J.; Zhu, M.; Meng, R.; Qin, H.; Peng, X. Ideal CdSe/CdS Core/Shell Nanocrystals Enabled by Entropic Ligands and Their Core Size-, Shell Thickness-, and Ligand-Dependent Photoluminescence Properties. *J. Am. Chem. Soc.* **2017**, *139* (46), 16556−67.
(18) Zhou, J.; Pu, C.; Jiao, T.; Hou, X.; Peng, X. A Two-Step Synthetic Strategy toward Monodisperse Colloidal CdSe and CdSe/CdS Core/Shell Nanocrystals. *J. Am. Chem. Soc.* **2016**, *138* (20), 6475−83.
(19) Gao, Y.; Peng, X. Photogenerated excitons in plain core CdSe nanocrystals with unity radiative decay in single channel: the effects of surface and ligands. *J. Am. Chem. Soc.* **2015**, *137* (12), 4230−5.
(20) Ma, X.; Tan, H.; Kipp, T.; Mews, A. Fluorescence enhancement, blinking suppression, and gray states of individual semiconductor nanocrystals close to gold nanoparticles. *Nano Lett.* **2010**, *10* (10), 4166−74.
(21) Ma, X.; Fletcher, K.; Kipp, T.; Grzelczak, M. P.; Wang, Z.; Guerrero-Martínez, A.; et al. Photoluminescence of Individual Au/CdSe Nanocrystal Complexes with Variable Interparticle Distances. *J. Phys. Chem. Lett.* **2011**, *2* (19), 2466−71.
(22) Kulakovich, O.; Strekal, N.; Yaroshevich, A.; Maskevich, S.; Gaponenko, S.; Nabiev, I.; Woggon, U.; Artemyev, M. Enhanced Luminescence of CdSe Quantum Dots on Gold Colloids. *Nano Lett.* **2002**, *2* (12), 1449−52.
(23) Lee, J.; Govorov, A. O.; Dulka, J.; Kotov, N. A. Bioconjugates of CdTe Nanowires and Au Nanoparticles: Plasmon-Exciton Interactions, Luminescence Enhancement, and Collective Effects. *Nano Lett.* **2004**, *4* (12), 2323−30.
(24) Brinson, B. E.; Lassiter, J. B.; Levin, C. S.; Bardhan, R.; Mirin, N.; Halas, N. J. Nanoshells Made Easy: Improving Au Layer Growth on Nanoparticle Surfaces. *Langmuir* **2008**, *24*, 14166−71.
(25) Hiramatsu, H.; Osterloh, F. E. pH-Controlled Assembly and Disassembly of Electrostatically Linked CdSe-SiO2 and Au-SiO2 Nanoparticle Clusters. *Langmuir* **2003**, *19*, 7003−11.
(26) Reimers, J. R.; Ford, M. J.; Marcuccio, S. M.; Ulstrup, J.; Hush, N. S. Competition of van der Waals and chemical forces on gold−sulfur surfaces and nanoparticles. *Nat. Rev. Chem.* **2017**, *1*, 1−12.
(27) Khon, E.; Hewa-Kasakarage, N. N.; Nemitz, I.; Acharya, K.; Zamkov, M. Tuning the Morphology of Au/CdS Nanocomposites through Temperature-Controlled Reduction of Gold-Oleate Complexes. *Chem. Mater.* **2010**, *22* (21), 5929−36.
(28) Demortiere, A.; Schaller, R. D.; Li, T.; Chattopadhyay, S.; Krylova, G.; Shibata, T.; et al. In situ optical and structural studies on photoluminesence quenching in CdSe/CdS/Au heterostructures. *J. Am. Chem. Soc.* **2014**, *136* (6), 2342−50.
(29) Carbone, L.; Nobile, C.; De Giorgi, M.; Sala, F. D.; Morello, G.; Pompa, P.; Hytch, M.; Snoeck, E.; Fiore, A.; Franchini, I. R.; Nadasan, M.; Silvestre, A. F.; Chiodo, L.; Kudera, S.; Cingolani, R.; Krahne, R.; Manna, L. Synthesis and Micrometer-Scale Assembly of Colloidal CdSe/CdS Nanorods Prepared by a Seeded Growth Approach. *Nano Lett.* **2007**, *7* (10), 2942−2950.
(30) Yu, W. W.; Qu, L.; Guo, W.; Peng, X. Experimental Determination of the Extinction Coefficient of CdTe, CdSe, and CdS Nanocrystals Chem. *Chem. Mater.* **2003**, *15*, 2854−60.
(31) van Huis, M. A.; Figuerola, A.; Fang, C.; Béché, A.; Zandbergen, H. W.; Manna, L. Chemical Transformation of Au-Tipped CdS Nanorods into AuS/Cd Core/Shell Particles by Electron Beam Irradiation. *Nano Lett.* **2011**, *11*, 4555−61.
(32) Xue, C.; Birel, O.; Gao, M.; Zhang, S.; Dai, L.; Urbas, A.; et al. Perylene Monolayer Protected Gold Nanorods: Unique Optical, Electronic Properties and Self-Assemblies. *J. Phys. Chem. C* **2012**, *116* (18), 10396−404.
(33) Tang, X.; Kroger, E.; Nielsen, A.; Strelow, C.; Mews, A.; Kipp, T. Ultrathin and Highly Passivating Silica Shells for Luminescent and Water-Soluble CdSe/CdS Nanorods. *Langmuir* **2017**, *33* (21), 5253−60.
(34) Zeng, B.; Palui, G.; Zhang, C.; Zhan, N.; Wang, W.; Ji, X.; et al. Characterization of the Ligand Capping of Hydrophobic CdSe−ZnS Quantum Dots Using NMR Spectroscopy. *Chem. Mater.* **2018**, *30* (1), 225−38.
(35) Pradhan, S.; Xu, L.; Chen, S. Janus Nanoparticles by Interfacial Engineering. *Adv. Funct. Mater.* **2007**, *17* (14), 2385−92.
(36) Yang, G.; Hallinan, D. T. Gold Nanoparticle Monolayers from Sequential Interfacial Ligand Exchange and Migration in a Three-Phase System. *Sci. Rep.* **2016**, *6*, 35339.
(37) Park, Y. K.; Park, S. Directing Close-Packing of Midnanosized Gold Nanoparticles at a Water/Hexane Interface. *Chem. Mater.* **2008**, *20*, 2388−93.
(38) Yang, G.; Chang, W. S.; Hallinan, D. T., Jr. A convenient phase transfer protocol to functionalize gold nanoparticles with short alkylamine ligands. *J. Colloid Interface Sci.* **2015**, *460*, 164−72.
(39) Lee, Y.; Jang, J.; Yoon, J.; Choi, J. W.; Choi, I.; Kang, T. Phase transfer-driven rapid and complete ligand exchange for molecular assembly of phospholipid bilayers on aqueous gold nanocrystals. *Chem. Commun. (Cambridge, U. K.)* **2019**, *55* (22), 3195−8.
(40) Yang, S.; Chai, J.; Song, Y.; Fan, J.; Chen, T.; Wang, S.; et al. In Situ Two-Phase Ligand Exchange: A New Method for the Synthesis of Alloy Nanoclusters with Precise Atomic Structures. *J. Am. Chem. Soc.* **2017**, *139* (16), 5668−71.

https://dx.doi.org/10.1021/acs.cgd.0c00582
Cryst. Growth Des. 2020, 20, 5890−5895